Mode shape reconstruction of an impulse excited structure using continuous scanning laser Doppler vibrometer and empirical mode decomposition

Yongsoo Kyong, Daesung Kim, Jedol Dayou,[a] Kyihwan Park, and Semyung Wang[b]
Department of Mechatronics, School of Information and Mechatronics Engineering, Gwangju Institute of Science and Technology, 1 Oryong-dong, Buk-gu, Gwangju 500-712, Republic of Korea

(Received 29 January 2008; accepted 22 May 2008; published online 3 July 2008)

For vibration testing, discrete types of scanning laser Doppler vibrometer (SLDV) have been developed and have proven to be very useful. For complex structures, however, SLDV takes considerable time to scan the surface of structures and require large amounts of data storage. To overcome these problems, a continuous scan was introduced as an alternative. In this continuous method, the Chebyshev demodulation (or polynomial) technique and the Hilbert transform approach have been used for mode shape reconstruction with harmonic excitation. As an alternative, in this paper, the Hilbert–Huang transform approach is applied to impact excitation cases in terms of a numerical approach, where the vibration of the tested structure is modeled using impulse response functions. In order to verify this technique, a clamped-clamped beam was chosen as the test rig in the numerical simulation and real experiment. This paper shows that with additional innovative steps of using ideal bandpass filters and nodal point determination in the postprocessing, the Hilbert–Huang transformation can be used to create a better mode shape reconstruction even in the impact excitation case. © *2008 American Institute of Physics.* [DOI: 10.1063/1.2943416]

I. INTRODUCTION

Vibration phenomena are important considerations in the design of machines, structures, instruments, and so on. Both the analysis and measurement of vibration are particularly important tasks because they should be performed together for the modeling of a real structure. A good vibration model has the potential capacity for allowing further engineering processes such as optimization. Among the many available measurement devices, the accelerometer is the most widely used sensor. With accelerometers and excitation such as the force from impact hammers or electromagnetic shakers, vibration characteristics can be calculated by the modal parameter estimation technique.[1]

Although the accelerometer has good sensitivity especially in high frequency bands, it has some limitations. Because of its nature as a contacting device, it can lead to mass loading especially for the measurement of light structures. If the structure is heavy, the accelerometer is still suitable but it cannot be attached to the rotating surface directly. In addition, for mode shape measurements, many accelerometers need to be attached in order to measure all spatial points. In this case, it will take some time to attach the accelerometers. For hammer roving tests, it also takes a long time to hit every measurement point.

Because of these limitations, in recent years noncontact measuring instruments such as laser Doppler vibrometer (LDV) have been more widely used.[2] Compared to conventional contact devices, LDV does not suffer from mass loading effects, and also reduces the setting time of sensors required for vibration testing.[2] These improvements have been helpful for engineers to shorten measurement time, and enhance the spatial accuracy of measurements. LDV is definitely faster than humans for testing, but when the structure is more complex, the testing process can still be time consuming.[3]

Many applications require spatially dense measurement. With conventional sensors such as accelerometers and discrete SLDV, the number of measurement points needs to be quite large in order to cover the whole area of a structure. This can take a relatively long time and requires a large storage capacity. As an alternative to the discrete scanning method, a continuous scanning method is introduced and is referred to in this paper as a continuous SLDV (CSLDV).

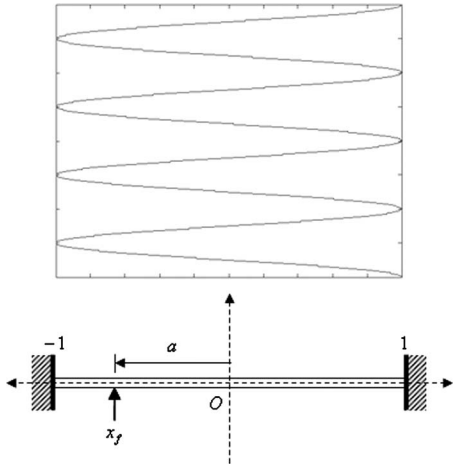

FIG. 1. Clamped-clamped beam with nondimensionalized coordinates and scan profile.

[a]Also at Vibration and Sound Research Group (VIBS), School of Science and Technology, Universiti Malaysia Sabah, Locked Bag 2073, 88999 Kota Kinabalu, Sabah, Malaysia.
[b]Electronic mail: smwang@gist.ac.kr.

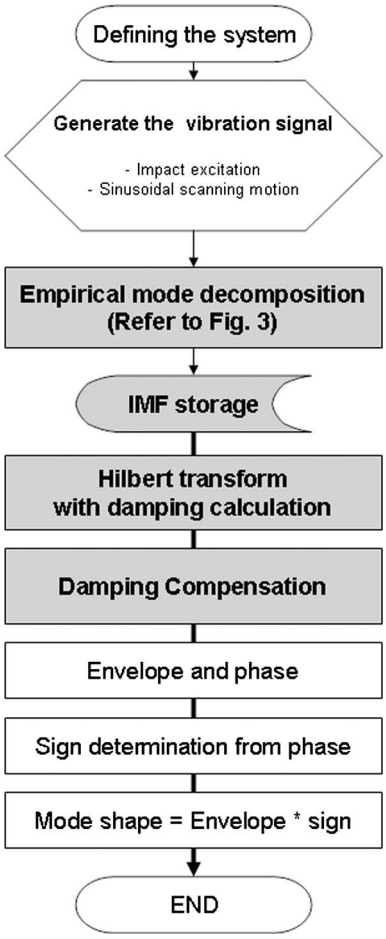

FIG. 2. Flowchart of mode shape reconstruction using the Hilbert–Huang transform approach with scanned data from impact testing including damping compensation.

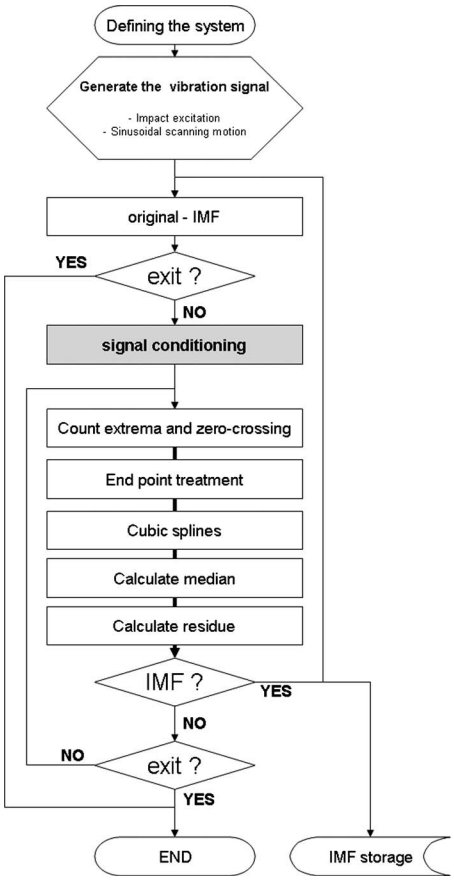

FIG. 3. Flowchart of empirical mode decomposition referred to Fig. 2 with scanned data from impact testing.

CSLDV is able to realize modal parameter estimation with only one measurement. In terms of a "continuous" scanning method, many scanning schemes are available, such as the short linear scan, the circular scan, the conical scan, and the straight line scan.[2–4] Specifically, in the sinusoidal scan, the Chebyshev demodulation has been introduced by Sriram *et al.*;[5] who have suggested the demodulation technique as a postprocessing technique to obtain the mode shapes of the vibrating structure.[5–7] The resultant mode shapes are approximated as a polynomial form.[2–10] According to this technique, approximated functional forms of natural mode shapes can be obtained based on the assumption of stationary velocity distribution.

However, because the Chebyshev demodulation technique is based on discrete Fourier transform analysis, periodicity conditions should be satisfied. Also leakage problems can degrade the results. In response to these problems, Kang *et al.*[11] suggested an alternative method called the Hilbert transform approach. Their work investigated the Hilbert transform for the demodulation of CSLDV output, and the deflection shape can be measured accurately. For the case of single frequency excitation, they obtained good experimental results. However, there was no investigation about the general excitation method, in, for example, impact and random excitation. This is because Hilbert transform alone cannot be used for the general excitation cases.

In this paper, Hilbert–Huang transform (HHT) technology[12] is proposed in order to realize the mode shape reconstruction for general excitation schemes. HHT has proved to be capable of analyzing nonlinear and nonstationary signals, and has been recently used in speech communication applications. This algorithm has also been used in a wide range of diverse fields: geological sciences, fluid dynamics, financial predictions, speech analysis, vibration analysis, and so on. This method is the combination of empirical mode decomposition (EMD) and the Hilbert transform. It can decompose a signal in the frequency-time domain.[12–15] After decomposition, modal responses can be obtained for the reconstruction of mode shapes using the Hilbert transform. In order to improve the quality of mode shape reconstruction, this paper proposes two additional steps for the postprocessing technique; the ideal bandpass filter in the EMD process and the instantaneous frequency for the determination of the nodal points of the structure. Also included in this paper are the results of the numerical simulation and real experiment performed for the validation of this technique.

II. SYSTEM MODELING

A. Sinusoidal continuous scanning LDVs

CSLDV technology can be used on many types of structures. However, for simplicity of discussion in this paper, a one-dimensional (1D) structure is used. Suppose that a 1D structure is scanned, and the velocity variation of the struc-

TABLE I. Dimensions and material properties of the clamped-clamped beam.

Property name	Value
Density	7.65×10^{3} kg/m^{3}
Young's modulus	207 GPa
Width of cross section	30×10^{-3} m
Thickness of beam	1×10^{-3} m
Length of beam	455×10^{-3} m

ture is statistically stationary. The scanning direction can be denoted by the coordinate x and the scanning limits are nondimensionalized to ±1.

In this case, a laser beam reflected by a driving mirror can be utilized as the measuring sensor, with sensor location defined as

$$x(t)=\cos(\Omega t), \tag{1}$$

where Ω is the laser scanning frequency, which is the same as the mirror driving frequency.

B. 1D sinusoidal scan with impact excitation

For this case, by applying the modal approach, the time varying velocity can be derived from the impulse response function as

$$v(x_o,t)=\sum_{q=1}^{Q}Y_q(\omega)\phi_q(x_f)\phi_q(x_o)$$
$$=\sum_{q=1}^{Q}\left[-\frac{\omega_{n,q}}{m\omega_{d,q}}e^{-\zeta_q\omega_{n,q}t}\sin(\omega_{d,q}t-\varphi)\right]\phi_q(x_f)\phi_q(x_o), \tag{2}$$

where Q is the number of considering modes; m is the mass; $Y(\omega)$ is the structural modal mobility; and $\phi_q(x_o)$ and $\phi_q(x_f)$ denote the couplings of the qth mode shape with the observing position x_o and the excitation position x_f, respectively.

Assuming that the structure is a clamped-clamped beam, the parameters for the velocity profile are determined, e.g., natural frequency $\omega_{n,q}$, damped natural frequency $\omega_{d,q}$, couplings of the qth mode shape, the weighted natural frequencies β_qL, the mode shape coefficients σ_q, and so on, as given in the vibration textbook.[16]

$$\omega_{d,q}=\omega_{n,q}\sqrt{1-\zeta^2}$$

$$\phi_q(x_f)=\cosh\beta_qx_f-\cos\beta_qx_f-\sigma_q(\sinh\beta_qx_f-\sin\beta_qx_f)$$

$$\phi_q(x_o)=\cosh\beta_qx_o-\cos\beta_qx_o-\sigma_q(\sinh\beta_qx_o-\sin\beta_qx_o). \tag{3}$$

As has been previously mentioned, the scanning limits are nondimensionalized to be ±1; hence, some coordinates have to be modified for the signal generation[17] which are

$$x_f=\frac{L}{2}(a+1)$$

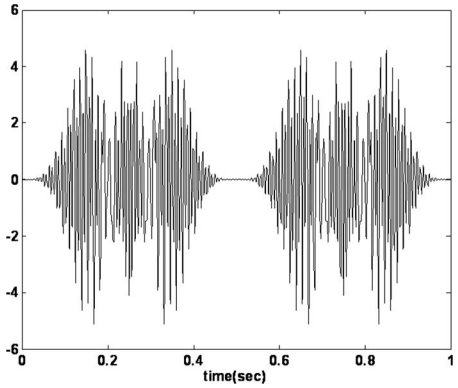

FIG. 4. Generated velocity signal for impact excitation with CSLDV.

$$x_o=\frac{L}{2}(\cos\Omega t+1), \tag{4}$$

where a is the nondimensionalized forcing position of the structure, as shown in Fig. 1. Finally, the velocity signal can be expressed by combining Eqs. (2)–(4).

III. THE HHT APPROACH FOR CSLDV

The HHT consists of two major steps: EMD and the Hilbert transform seen in Fig. 2.

A. EMD (Ref. 12)

The EMD procedures decompose the measured velocity signal into several oscillating components called intrinsic mode function (c_j: IMF). The IMF has been newly introduced by Huang *et al.* and is defined as a function satisfying two conditions: (a) in the whole data set, the number of extrema and the number of zero crossings must either equal or differ at most by one; (b) at any point, the mean value of the envelope defined by the local maxima and the envelope defined by the local minima is zero.[12] The first condition ensures the signs of the extrema: the local maxima are always positive while the local minima are negative.[13] For the second condition, although many researchers have studied and suggested the appropriate method to implement it, the recent development of Huang *et al.* does not include the implementation of the second condition.[14]

Kizhner *et al.* have detailed the algorithm for the EMD process.[14] The run-configuration vector is used in this process. This vector consists of several parameters: the sampling time interval, the maximum number of allowable IMFs, the maximum allowable number of EMD sifts for one IMF, and the pattern prediction option. His recently developed algorithm is composed of many steps: (a) EMD algorithm entry point, (b) EMD sifting process iterative loop entry point, (c) extend, (d) spline, (e) form the median, (f) form the running residue, (g) the IMF criteria check, and (h) process completion criteria check. Details can be found in their paper. From this point, EMD procedures are explained in detail, as shown in Fig. 3.

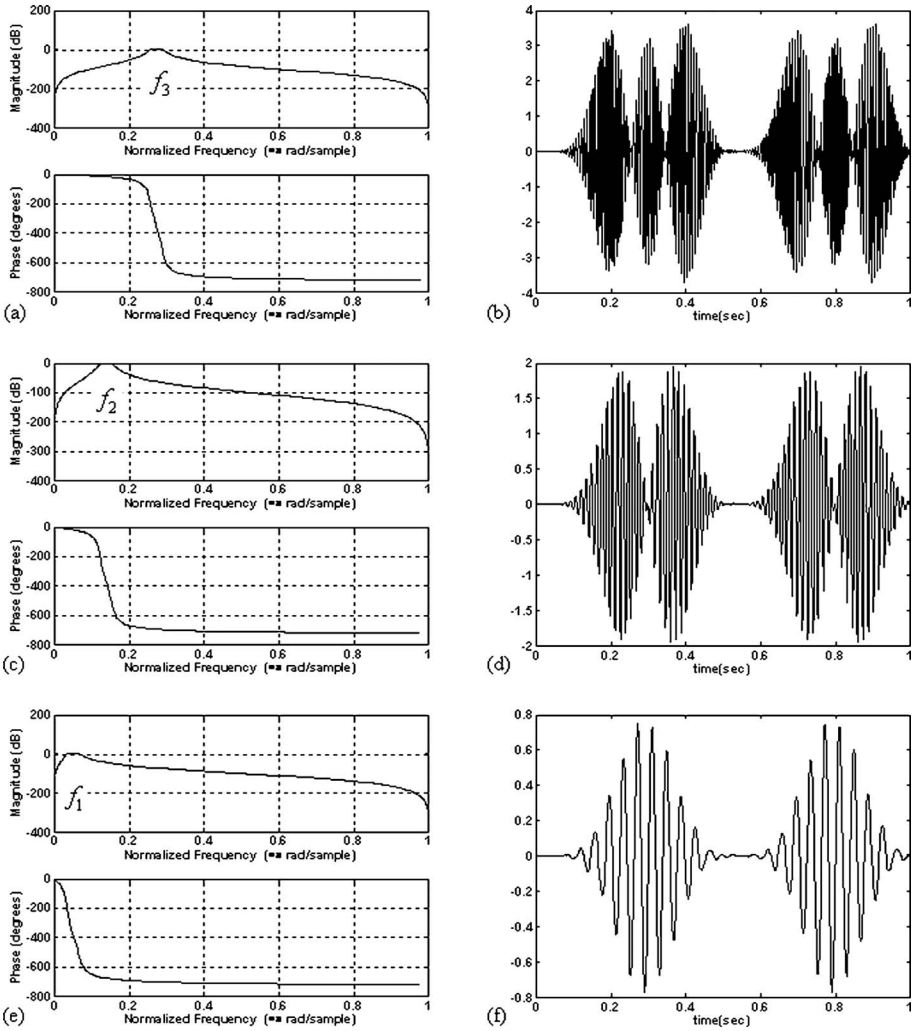

FIG. 5. Forth order Butterworth bandpass filter for third natural mode (a), filtered signal for third natural mode (b), for second mode [(c) and (d)], for first mode [(e) and (f)].

1. Signal conditioning for EMD

Signal conditioning can enhance the properties of vibration signals. Therefore it should be done in advance before signal analysis, as shown by the shaded box in Fig. 3. For the preliminary step, from the Fourier spectrum of the original signal, the approximated natural frequencies can be obtained and then the frequency ranges can be determined in advance.

Bandpass filtering. From the Fourier spectrum of the original signal, the approximated natural frequencies can be obtained and then the frequency bands for the filters can be determined. Yang *et al.* noted that if the modal frequencies are high and the signal has a high level of noise, bandpass filtering can be a good alternative. After filtering the data, the filtered data will be processed through EMD, and the resulting first IMF is more similar to the one of modal responses of the system.[15]

2. The IMF criteria check

The number of extrema points in the residue signal $E[\,r(t_i)\,]$ and the number of its zero crossings $Z[\,r(t_i)\,]$ have to satisfy the condition as expressed in Eq. (5) below. That is that the IMF must have more than 3 extrema and the difference of the number of extrema and zero crossings is not more than 1.

$$\{E[r(t_i)] > 3\} \text{ AND } \{|E[r(t_i)] - Z[r(t_i)]| \leqslant 1\}, \quad i \in \{1, \cdots, N\}. \tag{5}$$

If the residue signal satisfies the condition, the residue signal will be stored in an IMF matrix and then subtracted from the original signal. The subtracted signal will be the input signal of the sifting process iteratively.

3. Process completion criteria check

If the residue signal is not an IMF, it will be checked again for the exit criteria in Eq. (6). If the number of extrema is smaller than 4 or the number of IMF reaches the designated number of IMF in the run-configuration vector, the sifting process will be finished.

$$\{E[r(t_i)] \leqslant 3\} \text{ OR } \{\#\text{IMFs} = m\}. \tag{6}$$

In the original EMD process, the sifting process is continued until that the residue becomes a monotonic function. When the sifting process is repeated to obtain n IMFs, the resulting decomposition can be shown as

$$v(t) = \sum_{j=1}^{n} c_j + r, \tag{7}$$

where c_j is the jth intrinsic mode function and r is the residue. These IMFs, however, contained more than one fre-

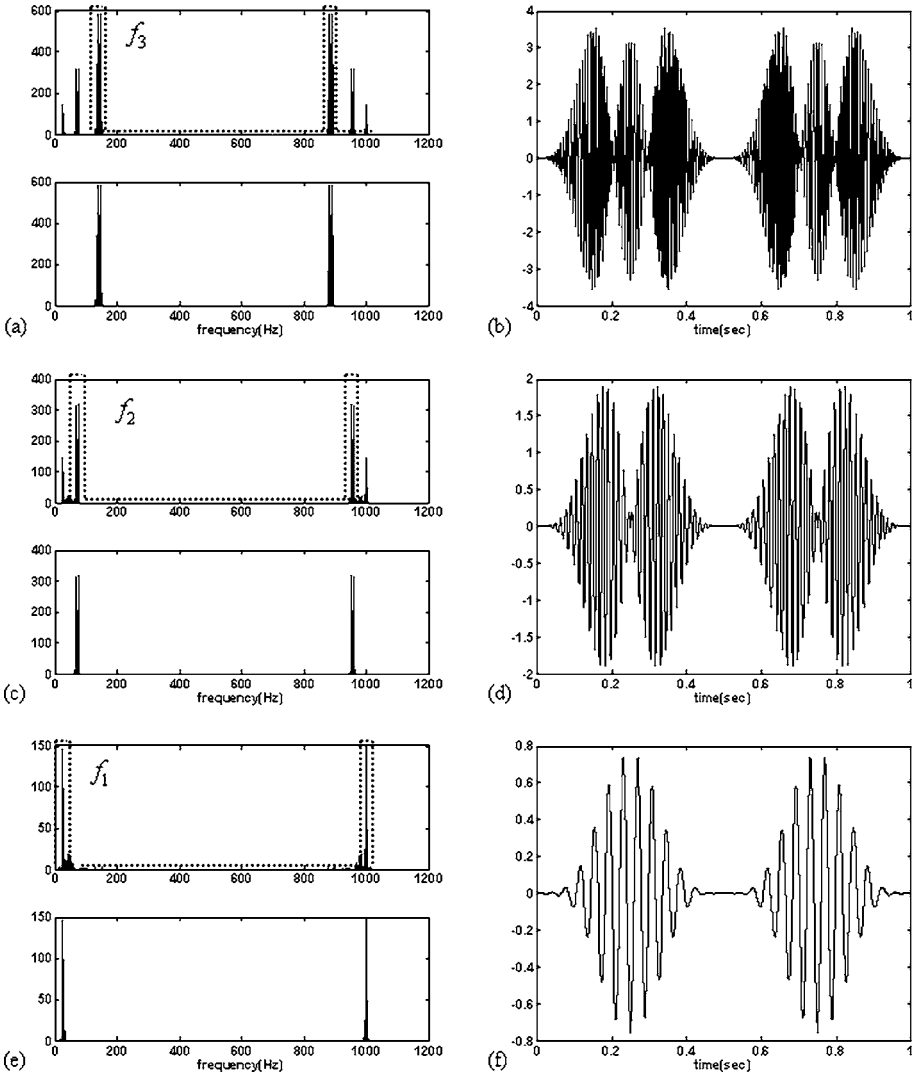

FIG. 6. Ideal bandpass filtering technique. First bandpass filter (--) for third natural mode and filtered spectrum (a), filtered signal for third natural mode (b), for second mode [(c) and (d)], for first mode [(e) and (f)].

quency component, so they are not modal responses. Therefore signal conditioning is suggested for the calculation of modal responses of the original signal. After the sifting steps including the signal conditioning technique are finished, the signal will be decomposed with some modal responses, some IMFs, and residue as expressed in Eq. (8).

$$v(t) \approx \sum_{j=1}^{n} M_j + \sum_{j=1}^{m-n} c_j + r. \tag{8}$$

Each modal response M_j will be applied with the Hilbert transform. For a small damping ratio and high natural frequency, the modal properties can be obtained from its modal responses.

B. The Hilbert transform and its application to CSLDV

The Hilbert transform can be practically applied for engineering purposes. It can determine the damping ratio at resonances from the impulse response function, and also estimate the propagation time from the cross correlation function.[18]

Kang *et al.*[11] suggested a Hilbert transform based approach for the measurement of deflection shapes from scanned data. The CSLDV output is an amplitude-modulated vibration, thus the deflection shape can be derived from the envelope and phase of output velocity signals.

If $v(t)$ is the velocity output of CSLDV, $\tilde{v}(t)$ which is the Hilbert transform of $v(t)$ can be expressed below

$$\tilde{v}(t) \equiv H\{\, v(t)\,\}. \tag{9}$$

In order to calculate the envelope, an analytic complex function $z(t)$ must be introduced,

$$z(t) = v(t) + j\tilde{v}(t) = E(t)e^{j\theta(t)}, \tag{10}$$

then one can get the envelope and the phase presented below.

$$E(t) = \sqrt{v^2(t) + \tilde{v}^2(t)}$$

$$\theta(t) = \tan^{-1}\left[\frac{\tilde{v}(t)}{v(t)}\right]. \tag{11}$$

With this information, the deflection mode shape can be plotted. The slope of the phase exhibits abrupt pulses at the node points, at which points the mode shape changes sign.[11]

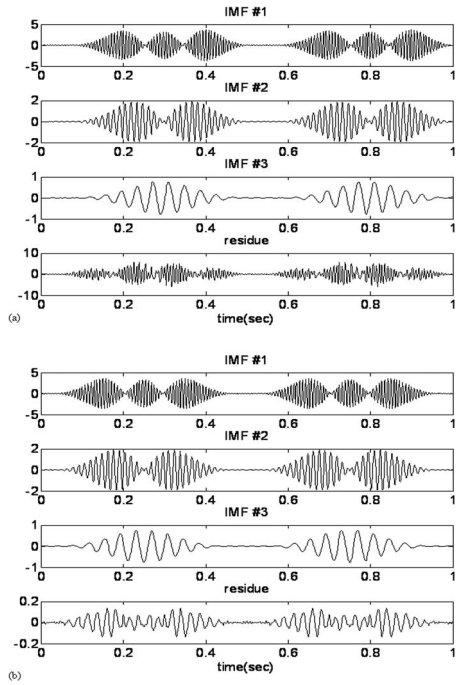

FIG. 7. Intrinsic mode functions as modal responses with conventional bandpass filtering (a), IMF and residue with ideal bandpass filtering (b).

IV. IMPROVED APPROACH OF HHT FOR CSLDV

A. Improvement in EMD (Ref. 12)

Yang *et al.* mentioned the bandpass filtering with an important note in their work.[15] They emphasized that the phase shift of the bandpass filter used should be as small as possible. In the following section of numerical simulation, the shifted signal will be discussed.

1. Signal conditioning for EMD

The bandpass filter makes the phase shift. If the signal has shifted, the resulting mode shape would be distorted because the coordinate of the mode shape is not matched to the scanning trajectory.[19] Also, the phase of the signal is important in order to decide the sign changes at nodal points. With the bandpass filter, the changes do not occur at the nodal point, which contribute to additional distortion in the reconstructed mode shape.

Ideal bandpass filtering.[20] In order to improve the quality of IMFs, the ideal bandpass filter is applied to the frequency response of the signal in the frequency domain as a postprocessing technique. The frequency components outside the bandpass filter are removed and then the velocity signal is reconstructed by the inverse Fourier transform. There will be no phase shift in the signal, unlike the case of the conventional bandpass filter.

B. Hilbert transform and CSLDV

1. Phase change criteria: the determination of nodal points

Kang *et al.*[11] mentioned the sign of the mode shape as discussed below. The slope of the instantaneous phase exhibits its abrupt pulses at the node points, at which points the deflection curve changes sign.

In the fundamentals of the Hilbert transform, the analytic signal has to be constructed to calculate the envelope and the phase. If the structure is excited sinusoidally with a certain mode shape $\Phi(x)$, the instantaneous frequency can be calculated from the phase, as described in Eqs. (12)–(14).

$$v(t) = \Phi(x)\cos\,\omega_d t, \tag{12}$$

$$\theta(t) = \tan^{-1}\left[\frac{\tilde{v}(t)}{v(t)}\right] = \tan^{-1}\left[\frac{\Phi(x)\sin\,\omega_d t}{\Phi(x)\cos\,\omega_d t}\right]$$

$$= \tan^{-1}[\tan\,\omega_d t] = \omega_d t, \tag{13}$$

$$\frac{d\theta(t)}{dt} = \frac{d}{dt}\{\,\omega_d t\,\} = \omega_d. \tag{14}$$

The abrupt changes in the phase plot become very distinguishable in the instantaneous frequency plot which is the differentiation of the phase. So the locations of sign changes can be calculated with the instantaneous frequency plot, and therefore the nodal points can be easily identified.

V. DAMPING COMPENSATION

In practice, for impact excitation, damping is always present with various magnitudes. In the time domain, the responses have exponential decay which causes the magnitudes of responses to decrease. The decrement of the magnitude of responses leads to a decrease in the magnitude of the envelopes strongly related to the mode shapes. Therefore, this damping should be compensated for, in order to achieve a good quality in the reconstruction of mode shapes.

For a special case in which the damping ratio ζ is very small and the natural frequency ω_n is large, Yang *et al.*[15] calculated the damped natural frequency ω_d from the slope of the phase $\theta(t)$, then obtained the damping ratio from the slope of the logarithm of envelope with the damped natural frequency, as described in Eqs. (15) and (16).

$$\ln E(t) = -\zeta\omega_d t + \text{constant}, \tag{15}$$

$$\omega_n(t) = \frac{d\theta(t)}{dt} = \omega_d. \tag{16}$$

Once we know the damping ratio, the mode shape can be compensated with the envelope of the response signal in the time domain, as shown in Eq. (17).

$$E'(t) = \frac{E(t)}{e^{-\zeta\omega_d t}}. \tag{17}$$

VI. NUMERICAL SIMULATION AND RESULTS

For validation of this technique, a clamped-clamped beam modeled as a continuous system is used, as shown in Fig. 1 and with required properties given in Table I. With these system properties, the first three natural frequencies are considered and calculated: 25.64, 71.21, and 139.57 Hz.

A. Parameters for digital signal processing

In digital signal processing, the required length of the sampled data is 2^b for an efficient fast Fourier transform where b is a certain integer. In order to obtain coefficients at

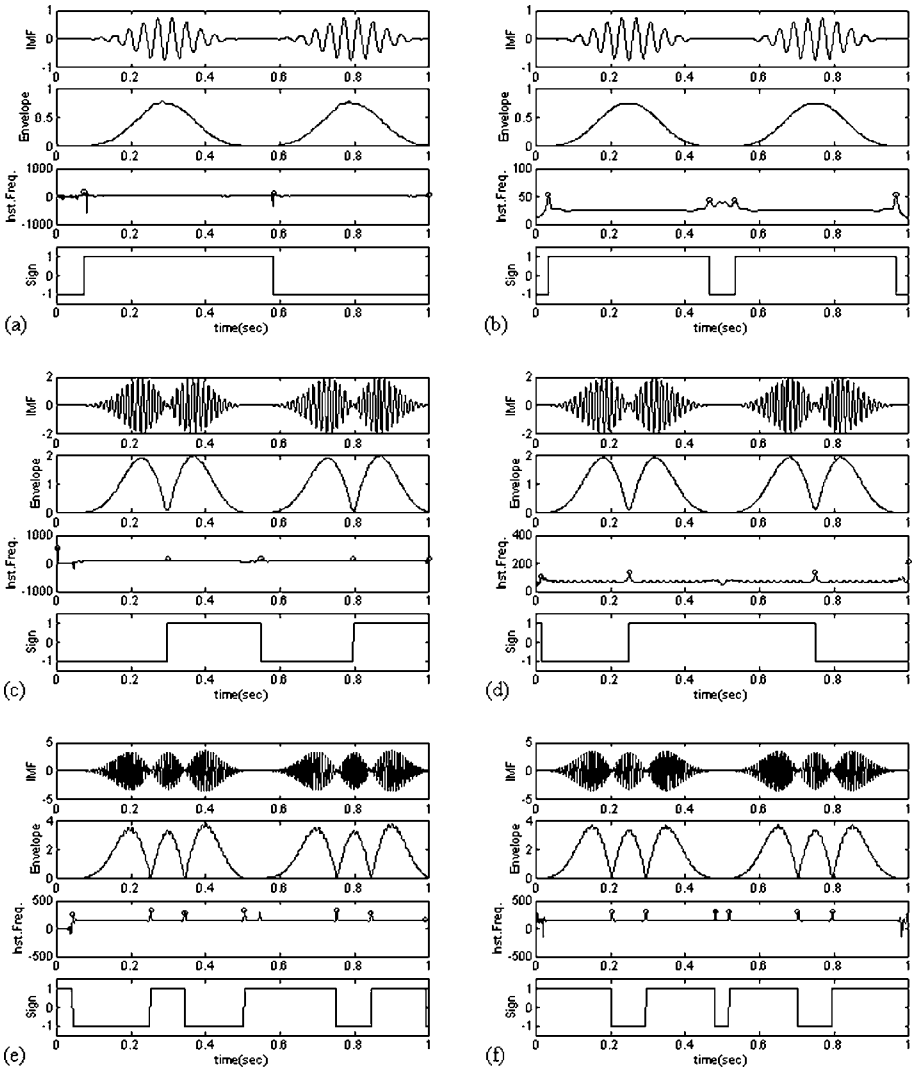

FIG. 8. Figures in the order of the process of mode shape reconstruction. IMF, its envelope, the instantaneous frequency, and determined sign with conventional bandpass filter of the first (a), the second (c), and the third modal responses (e), the same plots with the ideal bandpass filter of the first (b), the second (d), and the third modal responses (f).

certain frequencies, an appropriate resolution is required in the frequency range of interest. Here, for convenience, the sampling frequency is set to 2^b Hz for all cases.

B. Modal identification with scanned data from impact testing

For the numerical simulation of this paper, the impulse response function is used for generating a velocity profile. Mode shapes are then reconstructed from the velocity signal using the HHT approach. The procedure including the damping compensation is shown in Figs. 2 and 3 in the form of flowcharts, as previously discussed.

C. Validation of mode shape by using modal assurance criteria values

To evaluate how well the mode shape is reconstructed, modal assurance criteria (MAC) is used. This parameter is defined by

$$\mathrm{MAC(theory, calculated)} = \frac{|\{\phi_{\mathrm{calc}}\}^T\{\phi_{\mathrm{theor}}\}|^2}{(\{\phi_{\mathrm{calc}}\}^T\{\phi_{\mathrm{calc}}\})(\{\phi_{\mathrm{theor}}\}^T\{\phi_{\mathrm{theor}}\})}, \quad (18)$$

and this is a scalar quantity. This parameter is useful for quantifying the degree of correlation between a theoretical mode shape and a calculated mode shape.[1]

D. Results

1. For undamped case

Figure 4 shows the generated velocity signal from the impulse response functions. Signal conditioning techniques are used to improve the shape of the envelopes. With this velocity signal, a fourth order Butterworth bandpass filter is constructed and applied to each natural frequency band of the velocity signal, as shown in Fig. 5. As Yang *et al.*[15] found in their work, the time shift which can be thought as a phase shift, occurs at the beginning of the signal. As mentioned in Sec. IV A 1, the conventional bandpass filter has a phase-shifting problem which can confuse the sign determination and coordinate-trajectory matching. At the same time, the velocity will undergo the innovative suggestion, which is the ideal bandpass filter. The filter is applied in the frequency domain to filter out frequency components other than the natural frequency of interest, as shown in Fig. 6. For example, in Fig. 6(a), the filter is applied to remove f_1 and f_2 leaving f_3 and its sidebands, which is the interesting frequency components. The filter is applied over the natural

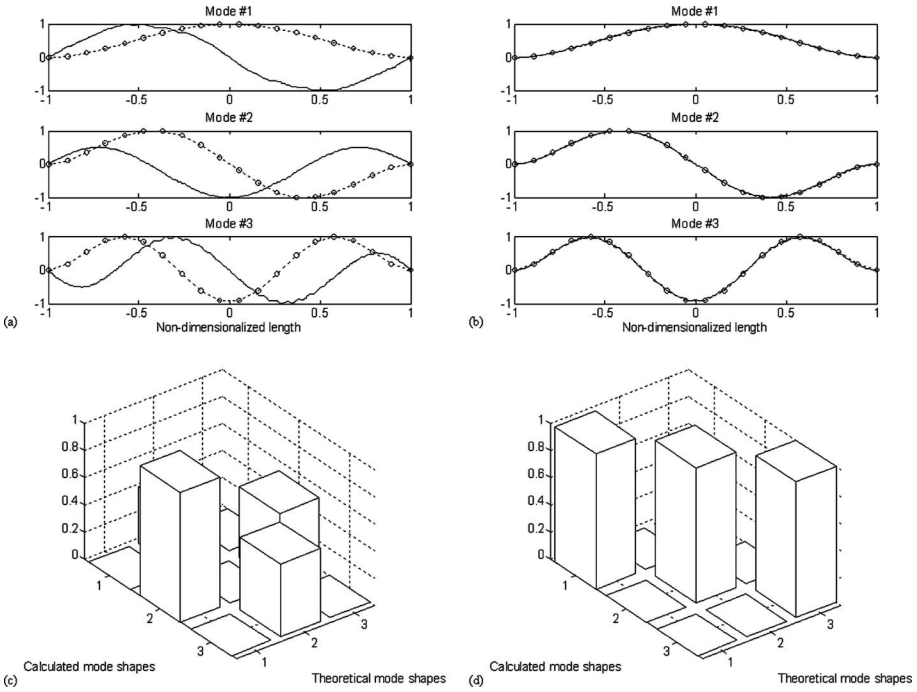

FIG. 9. Comparison between theoretical mode shapes (-o-) and calculated mode shapes (-) with conventional bandpass filter (a), the same as (a) with the ideal bandpass filter (b), MAC values of the vibration modes with bandpass filter (c), the same as (c) with the ideal bandpass filter (d).

frequency and the sidebands, and also to the mirroring components. The filtered signal shown at the bottom of Figs. 6(a), 6(c), and 6(e) will undergo the EMD process. As can be seen in Figs. 6(b), 6(d), and 6(f), the ideal bandpass filter is free from phase shifting contrary to the conventional bandpass filter in Figs. 5(b), 5(d), and 5(f).

After taking the HHT of the signal with both filtering techniques, Butterworth and the ideal, three IMFs are decomposed from its vibration signal, as shown in Fig. 7, corresponding to the three modal responses of the clamped-clamped beam. The higher frequency components are decomposed earlier than the lower frequency components through the EMD process.

The IMFs from the EMD process are used for the mode shape reconstruction, as shown in Fig. 8. In Figs. 8(a) and 8(b), for example, the figures are presented in the order of the procedure of the mode shape reconstruction for the first natural mode. In this figure, the plots on the left represent processing with the Butterworth filtered signal and those on the right are from the ideal bandpass filtered signal. The envelope and the instantaneous frequency can be obtained from the IMF given at the top of each figure. From the instantaneous frequency plots, abrupt changes can be obtained. These changes indicate the sign changes in mode shapes at the nodal points. By multiplying the envelope and sign changes, the mode shape can be calculated. From the instantaneous plots for both filtering techniques, the phase of the Butterworth case is shifted and distorted, especially in the middle, which is the location of the change in scanning direction from forward to backward. From the distortion of the phase, the sign of the reconstructed mode shape is determined but is incorrect, while the ideal bandpass case produces good results for mode shape reconstruction.

According to the results for the second and the third natural modes listed in Figs. 8(c)–8(f) with the application of the conventional bandpass filter, the shape of the envelopes are accurately obtained, but phase shifting leads to poor determination of the sign of the mode shape at the nodal points.

When the mode shape is expressed in the nondimensionalized domain which is matched with the scanning trajectory, the phase shifting causes negative effects on the mode shape reconstruction. With the shifted phase, the mode shape cannot be reconstructed accurately, as shown in Fig. 9(a). In Fig. 9(c), the MAC values show a poor correlation with the theoretical shape. Conversely the use of the ideal bandpass filter can make the reconstruction very accurate. It can be seen in Fig. 9(b) that with the ideal bandpass filter, the reconstructed mode shapes are very similar to the theoretical shapes, and

TABLE II. MAC values of the first three natural modes of a clamped-clamped beam for impact excitation by using the Hilbert-Huang transform approach with the ideal bandpass filter.

	Simulation					
	Conventional band pass filter			Ideal band pass filter		
	First	Second	Third	First	Second	Third
First theory	6.24×10^{-6}	0.414	2.18×10^{-5}	0.999	1.51×10^{-4}	1.66×10^{-4}
Second theory	0.959	8.63×10^{-5}	0.521	4.42×10^{-6}	0.999	5.09×10^{-5}
Third theory	5.23×10^{-8}	0.535	2.09×10^{-4}	2.22×10^{-4}	5.36×10^{-5}	0.999

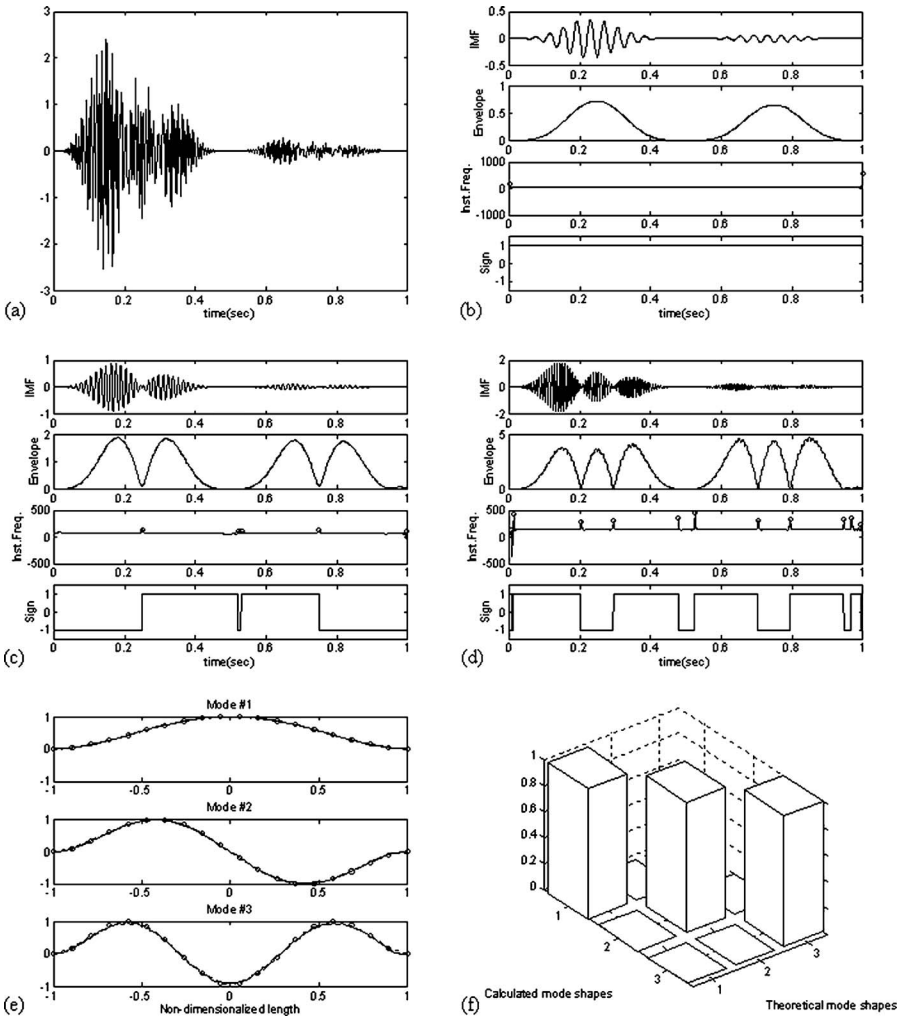

FIG. 10. Generated damped velocity signal (a), IMF, damping compensated envelope, the instantaneous frequency and determined sign of the first (b), the second (c), and the third modal responses (d), comparison between theoretical (-o-) and calculated mode shapes (-) (e), MAC values of the vibration modes (f). Damping ratios of each mode are 2%, 1%, and 0.5%.

therefore the MAC values are almost perfect for each mode, as shown in Fig. 9(d). Comparisons of the MAC numerical values in Table II further demonstrates the improvement in the quality of the mode shape reconstruction resulting from the application of the ideal bandpass filter.

2. For the damped case

If the structure is damped, the generated damped velocity is shown in Fig. 10(a). The damping ratios of the first three modes are 2%, 1%, and 0.5%. After the EMD process with an ideal bandpass filter, the first three natural modal responses are calculated. From each modal response, envelopes are obtained then damping is compensated using Eqs. (15) and (16). After the calculation of the instantaneous frequency, the sign of the mode shape is determined. Figure 10(b)–10(d) show the calculation procedures for the first, second, and third modal responses. According to Fig. 10(e), the compensated mode shapes are also similar to the theoretical mode shapes. Also the MAC values are almost perfect, as shown in Fig. 10(f) and Table III.

3. For the damped case with noise

In practice, speckle noise is always present in laser Doppler vibrometry. If the damping is high, the meaningful components of the vibration can be buried very quickly below the noise floor. By using the same damping ratios given

TABLE III. Comparisons of the damping compensation results with MAC values for the damped case and the noise case.

	Simulation					
	Damped			Damped with noise		
First	First	Second	Third	First	Second	Third
First theory	0.999	1.29×10^{-4}	1.53×10^{-4}	0.945	5.78×10^{-3}	2.12×10^{-3}
Second theory	8.06×10^{-6}	0.999	7.75×10^{-5}	2.26×10^{-2}	0.981	8.41×10^{-5}
Third theory	1.27×10^{-4}	5.18×10^{-5}	0.999	1.15×10^{-2}	7.66×10^{-4}	0.963

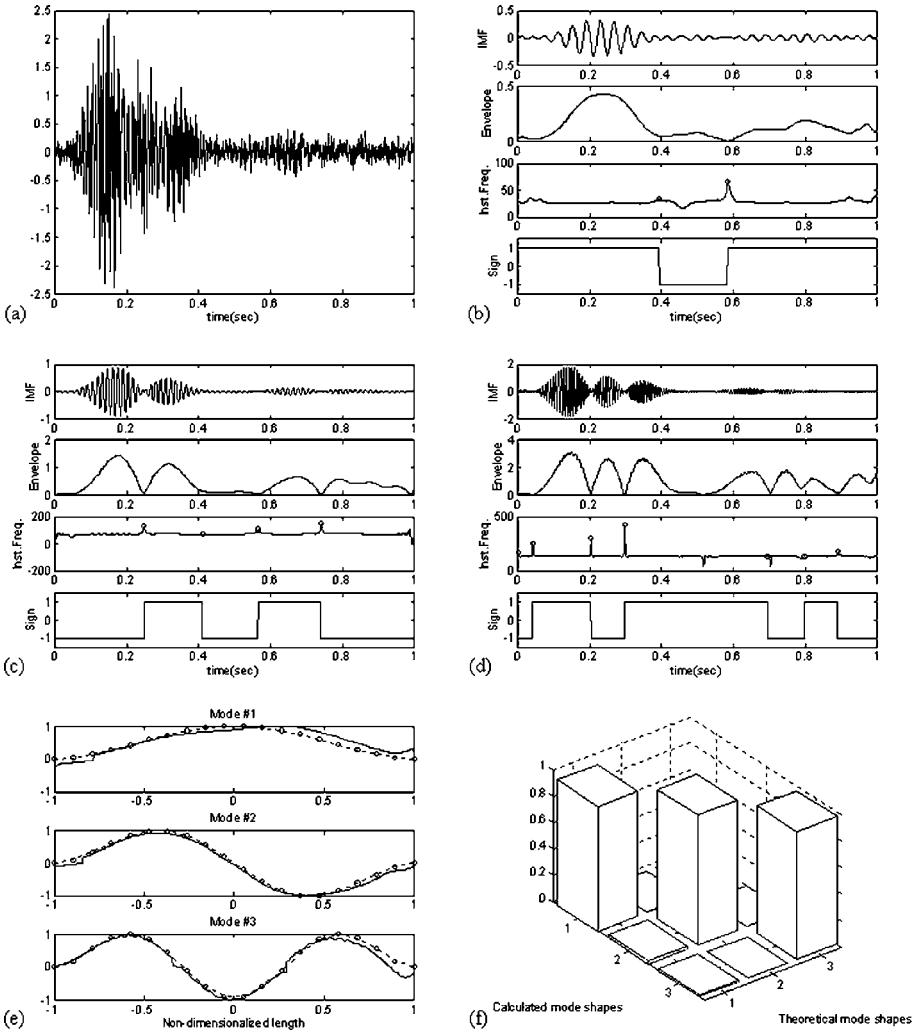

FIG. 11. Generated damped velocity signal with noise (a), IMF, damping compensated envelope, the instantaneous frequency, and determined sign of the first (b), the second (c), and the third modal responses (d), comparison between theoretical (-o-) and calculated mode shapes (-) (e), MAC values of the vibration modes (f). Damping ratios of each mode are 2%, 1%, and 0.5%.

in the previous section, the vibration signal is generated, as shown in Fig. 11(a). After half of the time span, the vibration components are buried below the noise floor. After the EMD process, however, the resulting modal responses are well decomposed and show the vibration modes. In Figs. 11(b)–11(d), the envelopes are obtained with some distortion at the end of each envelope. Noise causes this distortion but this can be resolved by spatial averages of mode shapes, as shown in Figure 11(e). Figure 11(f) and Table III also show good MAC values.

VII. REAL EXPERIMENT AND RESULTS

For the validation of this technique, a real experiment is carried out, for which Fig. 12 shows the schematic diagram. A clamped-clamped beam is tested in this experiment, the dimensions of which are given in Table I. The beam is scanned by a mirror which is controlled by a dSPACE controller board using the proportional-integral-derivative control method. While the laser is scanning the beam, the impulse excitation is given manually. The impact signal is triggered and acquired with the laser vibrometer's signal and the mirror scanning trajectory together, using a National Instrument data acquisition board and MATLAB. The scanning frequency is 5 Hz.

The vibration data resulting after acquisition using the mirror scanning trajectory are given in Fig. 13(a). In Fig. 13(a), the real mirror scanning trajectory (solid line) and the ideal sinusoidal scanning trajectory (dotted line) are shown. For ideal simulation cases, it is assumed that the laser can reach both clamped ends of the beam. In the experiment, the laser scans the inner region of the beam with some margin at both ends for accurate data acquisition. As a result, the scan looks shifted and the mode shape looks cut off in Fig. 13(e).

After the EMD process, with the modal responses, the

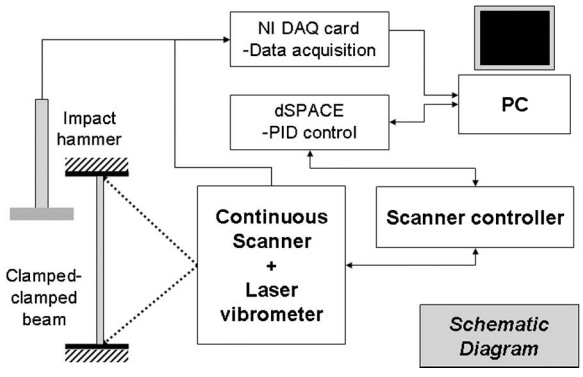

FIG. 12. Schematic diagram for the experiment using the continuous scanning laser Doppler vibrometer.

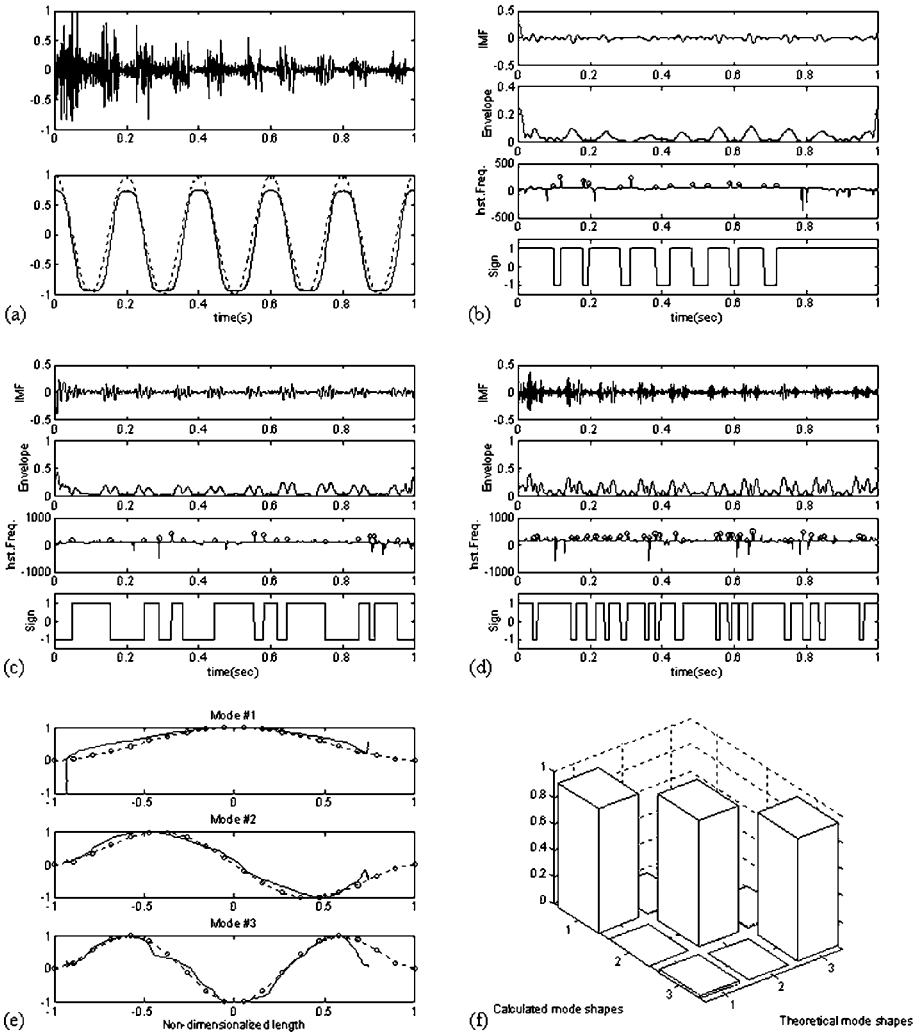

FIG. 13. Experimental velocity data with 5 Hz theoretical scanning trajectory (dotted) and real scanning trajectory (solid) (a), IMF, damping compensated envelope, the instantaneous frequency, and determined sign of the first (b), the second (c), and the third modal responses (d); comparison between theoretical (-o-) and calculated mode shapes (-) (e), MAC values of the vibration modes (f).

envelopes and instantaneous frequencies are obtained, and then the sign of the mode shapes are calculated, as shown in Figs. 13(b)–13(d). In Figs. 13(b)–13(d), the envelopes are more complicated than those in the simulation results. This complexity of shapes comes from the damping and the noise effect, as briefly shown in Figs. 11(b)–11(d) for the damped case with noise. However, this problem can be resolved through spatial averaging which is performed scan by scan.

Figure 13(e) shows the comparison of mode shapes between the theoretical and experimental results. In the experiment, the scanning mirror is paused at both ends for a very short period. However, during this period, the velocity data are measured. Therefore, mode shapes calculated at both ends appear to be shifted, and the end is cut off. In spite of the scanning problems, the mode shapes calculated are relatively accurate except at both ends. As shown in Fig. 13(f) and Table IV, the calculated mode shapes are well correlated to the theoretical mode shapes.

TABLE IV. Validation of the experimental results with MAC values.

	Experimental		
First	First	Second	Third
First theory	0.935	5.51×10^{-3}	6.03×10^{-3}
Second theory	8.57×10^{-5}	0.954	8.93×10^{-3}
Third theory	2.09×10^{-2}	9.02×10^{-4}	0.923

VIII. SUMMARY

The HHT approach has been investigated in this paper for the reconstruction of the mode shapes of a structure which has been excited using impact force. For all the cases, such as undamped, damped, damped with noise, and the real experiment, it was shown that the HHT approach can give good demonstrated results in comparison with theory. To further improve the mode shapes' quality, the ideal bandpass filter and the instantaneous frequency methods were proposed as a postprocessing technique. Visual inspections of the mode shapes and comparison of their MAC values show that the improved HHT approach gives the accurate mode shapes with respect to the theoretical prediction.

[1] D. J. Ewins, *Modal Testing: Theory and Practice*, 2nd ed. (Research Studies, England, 2000).
[2] P. Castellini, G. M. Revel, and E. P. Tomasini, Shock Vib. **30**, 443 (1998).
[3] M. Martarelli, Ph.D. thesis, University of London, 2001.
[4] A. B. Stanbridge and D. J. Ewins, Mech. Syst. Signal Process. **13**, 255 (1999).
[5] P. Sriram, S. Hanagud, J. Craig, and N. M. Komerath, Appl. Opt. **29**, 2409 (1990).

[6] P. Sriram, S. V. Hanagud, and J. I. Craig, AIAA J. **30**, 765 (1992).
[7] P. Sriram, S. Hanagud, and J. I. Craig, Int. J. Anal. Exp. Modal Anal. **7**, 169 (1992).
[8] A. B. Stanbridge and D. J. Ewins, Proceedings of the IMAC XIV, 1996 (unpublished), pp. 816–822.
[9] A. B. Stanbridge, M. Martarelli, and D. J. Ewins, Proceedings of the IMAC XVII, 1999 (unpublished), pp. 986–991.
[10] A. B. Stanbridge, A. Z. Khan, and D. J. Ewins, Shock Vib. **7**, 91 (2000).
[11] M. S. Kang, A. B. Stanbridge, T. G. Chang, and H. S. Kim, Mech. Syst. Signal Process. **16**, 201 (2002).
[12] N. E. Huang, Z. Shen, S. R. Long, M. C. Wu, H. H. Shih, Q. Zheng, N.-C. Yen, C. C. Tung, and H. H. Liu, Proc. R. Soc. London, Ser. A **454**, 903 (1998).
[13] M. Dätig and T. Schlurmann, Ocean Eng. **31**, 1783 (2004).
[14] S. Kizhner, K. Blank, T. Flatley, N. E. Huang, D. Petrick, and P. Hestnes, IEEEAC Paper No. 1345, Version 2, Updated 18 November 2005.
[15] J. N. Yang, Y. Lei, S. Pan, and N. Huang, Earthquake Eng. Struct. Dyn. **32**, 1443 (2003).
[16] D. J. Inman, *Engineering Vibration*, 2nd ed. (Prentice-Hall, Englewood Cliffs, NJ, 2001).
[17] Y. Kyong, M.S. thesis, Gwangju Institute of Science and Technology, 2001.
[18] N. Thrane, J. Wismer, H. Konstantin-Hansen, and S. Gade, Practical use of the "Hilbert transform," Application Note, Bruel&Kjaer.
[19] Y. Kyong, S. Wang, J. La, K. Park, K. S. Kang, and K. S. Kim, Proceedings of Tenth International Congress on Sound and Vibration (ICSV), 2003 (unpublished), pp. 4393–4400.
[20] A. V. Oppenheim, R. W. Schafer, and J. R. Buck, *Discrete-Time Signal Processing*, 2nd ed. (Prentice-Hall, Englewood Cliffs, NJ, 1999), p. 44.